


RESEARCH ARTICLE

Hydrodynamic modeling of ephemeral flow in the lishana channel systems of the Cuvelai Basin—Northern Namibia

Robert Arendt¹  | Christian Reinhardt-Imjela¹ | Leona Faulstich¹ | Achim Schulte¹ | André Assmann² | Robert Jüpner³ | Petrina T. Johannes⁴ | Damas Alfred Mashauri⁴

¹Institute of Geographical Science, Applied Physical Science—Environmental Hydrology and Resource Management, Freie Universität Berlin, Berlin, Germany

²geomer GmbH, Heidelberg, Germany

³Department of Civil Engineering, Hydraulic Engineering and Water Management, Technical University of Kaiserslautern, Kaiserslautern, Germany

⁴Faculty of Engineering and Information Technology, Department of Civil and Environmental Engineering, University of Namibia, Ongwediva, Namibia

Correspondence

Robert Arendt, Department of Earth Science, Freie Universität Berlin, Berlin, Germany.
Email: robert.arendt@fu-berlin.de

Funding information

Deutsche Hydrologische Gesellschaft (DHG); Freie Universität Berlin

Abstract

The transboundary region of the lishana system in the western Cuvelai Basin, between southern Angola and northern Namibia, is frequently affected by floods at irregular intervals. As a result, the predominantly rural, subsistence farming population has experienced crop failures, human, and economic losses. To date, very little is known about the generation of floods, flood concentration, and stormwater drainage dynamics in this region. In this study, 2D-hydrodynamic modeling was applied to reconstruct one of the latest major flood events during the rainy season from November 2008 to March 2009 in order to study the runoff behavior and interconnectivity of the lishana system. The model focused on the eastern part of the lishana system, which was most affected by floods and flood damage due to the high population density in and around Oshakati, the regional capital. Two main streams were identified noteworthy because they merge and subsequently affect Oshakati. Regarding the simulated flood event water depths vary from 0.1 m to 14 m, with an average of 0.2 m, while water depths above 5 m were attributed to borrow pits. The inundation area ranged up to 1860 km² and the amount of water left after the rainy season on March 25th, 2009, was determined between 0.116 and 0.547 km³, depending on the amount of evapotranspiration considered in the model. Thus, in the Angolan part of the lishana system, significantly larger quantities of water are available for longer periods of time during the subsequent dry season, whereas the system in Namibia stores less water, resulting in a shorter water retention period.

KEYWORDS

flood, FloodArea11, SCS-CN, TanDEM-X, TRMM

1 | INTRODUCTION

This study focuses on the transboundary Cuvelai Basin between southern Angola and northern Namibia, specifically the lishana system (Figures 1 and 2). This area has been the major focus of a broader research project

dealing with the issues of floods, droughts, and water quantity and quality (Arendt et al., 2020, 2021; Faulstich et al., 2018). Ephemeral and endorheic river channels, also known as Oshana (plur. lishana), characterize this distinct region. They are shallow, net-like waterways with thousands of natural depressions and smaller pans embedded in the channel system

This is an open access article under the terms of the [Creative Commons Attribution-NonCommercial-NoDerivs](https://creativecommons.org/licenses/by-nc-nd/4.0/) License, which permits use and distribution in any medium, provided the original work is properly cited, the use is non-commercial and no modifications or adaptations are made.

© 2023 The Authors. *River Research and Applications* published by John Wiley & Sons Ltd.



FIGURE 1 Northern Namibia, border region, left: large shallow inundated areas, right: flooded sorghum fields of a kraal. [Color figure can be viewed at wileyonlinelibrary.com]

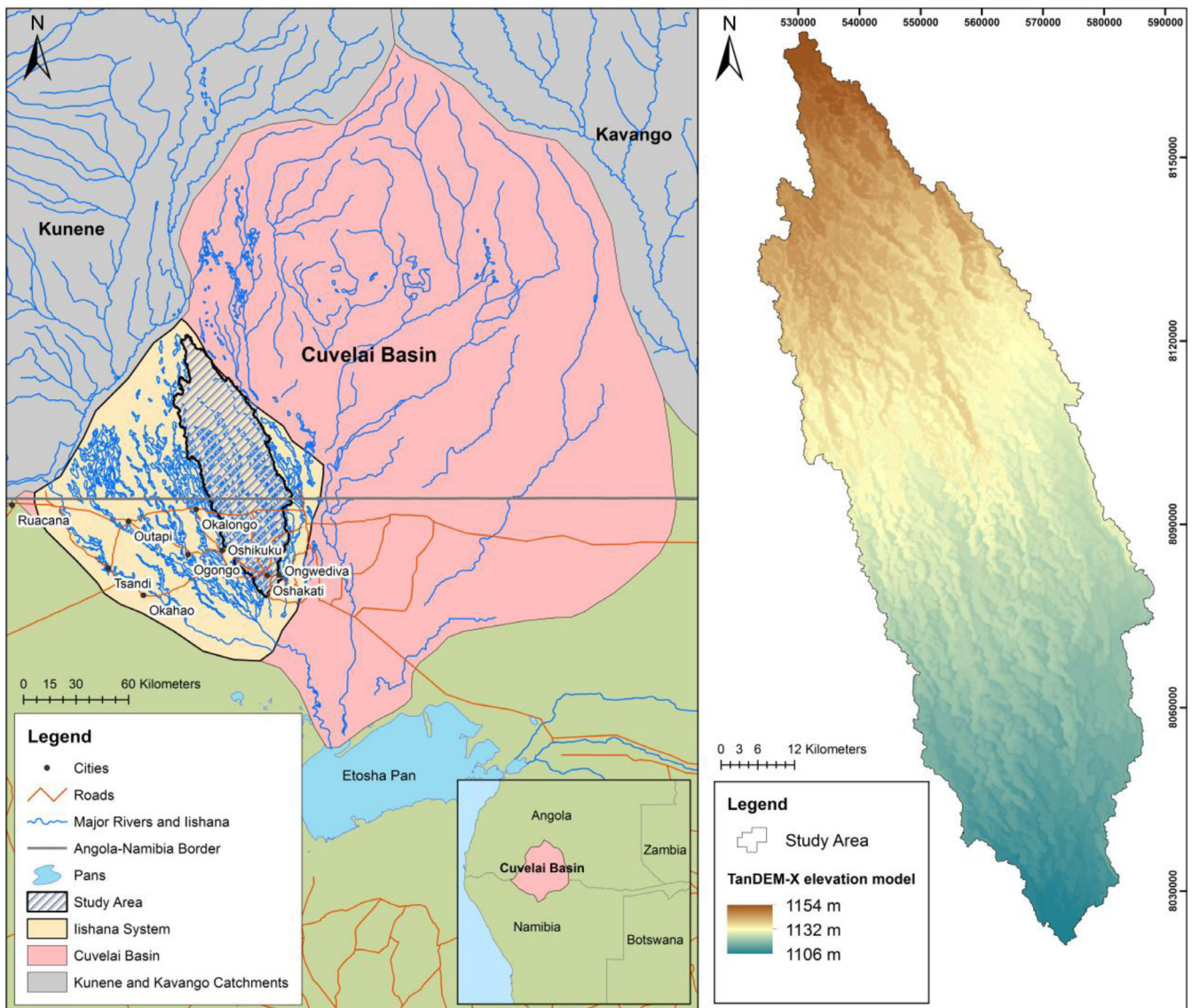


FIGURE 2 Map of the study area and elevation map. [Color figure can be viewed at wileyonlinelibrary.com]

(Awadallah & Tabet, 2015; Cunningham et al., 1992; Goormans et al., 2015; Kluge et al., 2008; Luetkemeier et al., 2017; Mendelsohn et al., 2013; Ngula Niipele & Chen, 2019; Persendt & Gomez, 2016; Shifidi, 2016; Zimmermann, 2013).

During the rainy season between November and March, small flood events typically replenish the channel system (Figure 1), which is greatly needed after a regular dry period. They bring fish, deliver water for agricultural, livestock, and domestic use and fill natural and artificial reservoirs (Arendt et al., 2021; Cunningham et al., 1992; Seely et al., 2003). In addition, floods in Namibia are intensified by local convective precipitation.

Nevertheless, drought events can occur when the rainy season is too weak. Such events transpire in the late 1980s and mid-1990s. In more recent years, very frequent droughts transpired between 2013 and 2019, with the exception of 2017 (Kerdiles et al., 2015; Luetkemeier et al., 2017; Seely et al., 2003). However, major flood events occurred in 2008, 2009, 2010, 2011 and 2013, causing fatalities, the loss of livestock and crop yield, and damage to property and technical infrastructure (Arendt et al., 2021; Awadallah & Tabet, 2015; Bischofberger et al., 2016; Filali-Meknassi et al., 2014; Mandl et al., 2013; Mufeti et al., 2013; Persendt et al., 2015; Shifidi, 2016; Skakun et al., 2013).

Different studies on the Cuvelai Basin have tried to reconstruct past flood events by mapping their extents via time series satellite images or the application of different sensors (radar and optical) (Awadallah & Tabet, 2015; De Groeve, 2010; Müller et al., 2018; Skakun et al., 2013). Most studies attempted to forecast the probable extent of a flood event and tried to identify areas of high risk, but this was typically accomplished using a very coarse spatial resolution. Moreover, some studies did not include the transboundary aspect of the basin or the lishana system (Awadallah & Tabet, 2015; De Groeve, 2010; Skakun et al., 2013). De Groeve (2010) established a real-time flood monitoring approach aiming to detect the beginning of flood events, but it provides no ability to predict further flood routing. Moreover, Mufeti et al. (2013) assembled a rainfall-runoff model for the 2009 flood event. The model provides no information about flood inundation, but it did estimate the streamflow output based on a 90 m resolution SRTM DEM (Shuttle Radar Topography Mission Digital Elevation Model).

The research by Goormans et al. (2015) reported the first approach to using hydrodynamic flood modeling coupled with a hydrological model in the lishana system. Focusing just on the boundary (approx. 20 km × 30 km) of the City of Oshakati (regional capital), they merged a 90 m resolution SRTM, a 50 m resolution DTM (Digital Terrain Model) generated from aerial photographs, and a 5 m × 5 m LiDAR DTM as a base for further calculations with InfoWorks RS v10.5 (Innovyze Ltd, UK). The study's aim was to calibrate the model with the help of the 2011 flood event. On that basis, they created a design flood to benchmark the local government's plans to construct a dike and diversion channel to protect the city of Oshakati against future floods.

In summary, analysis of the area has ranged from rapid satellite and topographical-based screening to a first, small-scaled hydraulic and hydrodynamic assessment (Awadallah & Tabet, 2015; De Groeve, 2010; Goormans et al., 2015; Müller et al., 2018; Skakun et al., 2013; Tyrna et al., 2018). However, there is no

2D-hydrodynamic assessment of the entire lishana system, nor is there a transferable model approach available yet.

It has been made clear that the lishana system is a unique inland delta, which serves as an important water source for the rural population. At the same time, the system has not yet been fully understood in terms of its flow processes and natural properties.

Therefore, the aim of this study was to generate information about flood routing in order to understand the interconnectivity of the lishana system as well as the related filling of the lishana depressions. Describing the runoff processes in the lishana system, the model outputs provide metrics about inundation depths at different times during the rainy season and the amount of water remaining at the season's end. The model can be used for scenario calculations of future floods.

2 | MATERIALS AND METHODS

2.1 | Study area

The study area is part of the lishana system located in the western part of the transboundary Cuvelai Basin (Figure 2). The lishana system covers an area of 18,370 km² and is characterized by a high population density (Mendelsohn et al., 2013). About 1.2 million people live in this area (34% in Angola and 66% in Namibia) (Mendelsohn & Weber, 2011; Persendt & Gomez, 2016). The study area itself is located in the eastern part of the lishana system and has an area of 4600 km². In the far south of the study area, the town of Oshakati represents the main developing center of the region.

The study area is semi-arid, being influenced by the cold Benguela Current and the Inner Tropical Convergence Zone (ITCZ). Precipitation increases from west to northeast from 350 to 950 mm a year. Evaporation rates increase along the same west-east gradient from 2600 to 3200 mm/a. The rainy season lasts from October to April, but it is most prominent from December/January to March. A high intra- and inter-annual variability in precipitation is characteristic, which in consequence regularly brings floods and droughts (Gaughan et al., 2016; Kundzewicz et al., 2013; Reason & Smart, 2015; Shifidi, 2016).

The topography is flat with an elevation of approx. 1100 m to 1200 m and a northwest-southeast gradient of only 0.5 ‰ to 1 ‰. The surface hydrology is dominated by a diffuse network of shallow endorheic and ephemeral channels (lishana), which run from northwest to southeast and ultimately drain in the Etosha Pan. The width of the lishana channels varies greatly from around 100 m to over 1750 m with depths ranging between 1 and 7 m (Mendelsohn et al., 2013). The elevated areas between the lishana consist of Kalahari sands. These areas are used for communal farming, crop production, and rain-fed agriculture (subsistence farming). The sediments of lower and intermediate lishana areas are dominated by aeolian and fluvial sediments (clay fraction), calcite, and silicate crusts (Faulstich et al., 2018; Goudie & Viles, 2015; Hipondoka, 2005; Hüser et al., 2001). Shallow natural pans have formed in these areas, which fill with water during sufficient local precipitation or flood events. At these times of inundation, the pans connect with each other to form a unique and characteristic inland delta (Arendt et al., 2021;

Hipondoka, 2005; Persendt & Gomez, 2016; Van Der Waal, 1991). The majority of surface water comes from the Angolan side of the transboundary region, with flood events often being amplified or intensified by local convective rainfall events.

2.2 | Hydrodynamic modeling

Two-dimensional (2D) hydraulic models are used for flood hazard mapping and to support flood risk management. They solve the shallow water equations and therefore require various input data such as a digital elevation model (DEM) and precipitation data, which are the most important datasets among others. The DEM is used to calculate flow directions and, together with surface roughness data (obtained from land use data), to calculate flow velocity (Tyrna et al., 2018).

For digital elevation data, a TanDEM-X model was used. It provides a spatial resolution of 12.5 m and a vertical accuracy of less than 2 m in very flat regions (Rizzoli et al., 2017). Before it could be used for hydrodynamic calculations, it was corrected by eliminating outliers and interferences due to backscatter effects from water surfaces or other inconsistencies. In addition, significant artificial objects below DEM spatial resolution were included, such as roads, dams, culverts, and bridges. The procedure for the DEM preprocessing is described by Arendt et al. (2020 & 2021), Wessel (2016) and Wendleder et al. (2013).

There are many different models available for a 2D-hydrodynamic simulation of flooding processes (Achleitner et al., 2020), such as HYDRO_AS-2D (Nujic, 2016), TELEMAC-2D (Ata, 2017), HEC-RAS 2D (Desalegn & Mulu, 2021), P-DWave (Leandro et al., 2014), JFolw (Bradbrook, 2006), and FloodArea (Tyrna et al., 2018). They all have their advantages and disadvantages and slightly differ from one another in what hydraulic equations are used, whether they are raster-grid or mesh-based, and if they are open-source, commercial, or freeware. Moreover, some of the models have a variety of additional functions, such as the ability to couple with an urban drainage system, or deeper modeling capabilities for runoff generation and vertical hydrological processes. In this study, the software package FloodArea11 was used. Developed by the geomer GmbH in Heidelberg (Germany), FloodArea11 is designed as an ArcGIS extension (geomer GmbH, 2017) and able to calculate water depth and flow velocity. The calculation of flow velocity is based on the Gauckler-Manning-Strickler equation for uniform flow (Manning, 1891; Strickler, 1923). The advantage of FloodArea for our study is its ability to implement temporally and spatially varying precipitation. A second major advantage is the computationally less demanding Manning-Strickler approach, which allows a simulation of large areas with a long continuous time series. The Manning-Strickler approach presumes that, under uniform conditions, the bottom slope (S) equals the slope of the energy grade line (Tyrna et al., 2018).

The average velocity (V) within the cells is calculated from the Strickler coefficient (K_{st}), which represents the surface roughness, the hydraulic radius (R_h), and the slope (S) according to equation 1:

$$V = K_{st} * R_h^{2/3} * S^{1/2} \quad (1)$$

To derive roughness coefficients, a supervised land use classification was produced based on a 10 m resolution Sentinel-2B image acquired in October 2017. With the help of the Maximum-Likelihood-Classifer six land use classes could be identified (water, savanna, lishana, gravel, forest, undefined). The land use class of savanna covers about 60% and forest is the second major class of about 30% while water and gravel strike with around 9%. Approximately 5% of all the forest class is attributed to Namibia. Later the land use classification had to be strongly generalized according to the 15 low-resolution precipitation tiles (each 25 km × 25 km) due to the TRMM rainfall data resolution (see Section 2.3). On this basis, Strickler roughness coefficients could be estimated using the standard table from Chow (1959). The discharge rate for each cell is calculated by multiplying the velocity (V) by the cross-sectional area of each pixel.

Flat topographies can lead to low flow velocities and high dispersion rates, which cause unrealistic inundation patterns. Therefore, FloodArea uses the D_∞ algorithm developed by Tarboton (1997) for flood routing. For this purpose, the flow direction is determined as the direction of the steepest slope on plain and triangular aspect and is expressed as a steady flow direction degree. Moreover, it distributes the flow to two neighboring cells and calculates the flow direction limited to 16 fixed angles. In this study, the hardware allowed for the calculation of 10 cores simultaneously and needed 24 days in total to complete the model run.

2.3 | Precipitation

For modeling the 2008/2009 rainy season, data from the Tropical Rainfall Measurement Mission (TRMM, “TMPA-RT Near-Real-Time Precipitation L3 day 0.25° × 0.25° V7”) was used. The study area is covered by 15 precipitation tiles. For each tile, a daily rainfall time series was generated from the raster data for the period between November 26, 2008, and March 25, 2009. The daily data were disaggregated, complying with the hourly modeling time steps required by FloodArea. Therefore, a uniform hydrograph assuming constant rainfall between 3 and 5 p.m. was used according to typical convective rain events close to the ITCZ (Figure 3).

2.4 | Runoff generation

FloodArea simulates the flood wave propagation in the channel system. For the transformation of rainfall into runoff the SCS-CN method (United States Department of Agriculture [USDA], 2009) was used (Figure 3 and Equation 2).

$$S = \frac{1000}{CN} - 10 \quad (2)$$

$$\begin{aligned} I_a &= S \times \lambda, \lambda = 0.1, \\ P > I_a &= S \times 0.1, \\ P &= 0; P < I_a = S \times 0.1 \end{aligned} \quad (3)$$

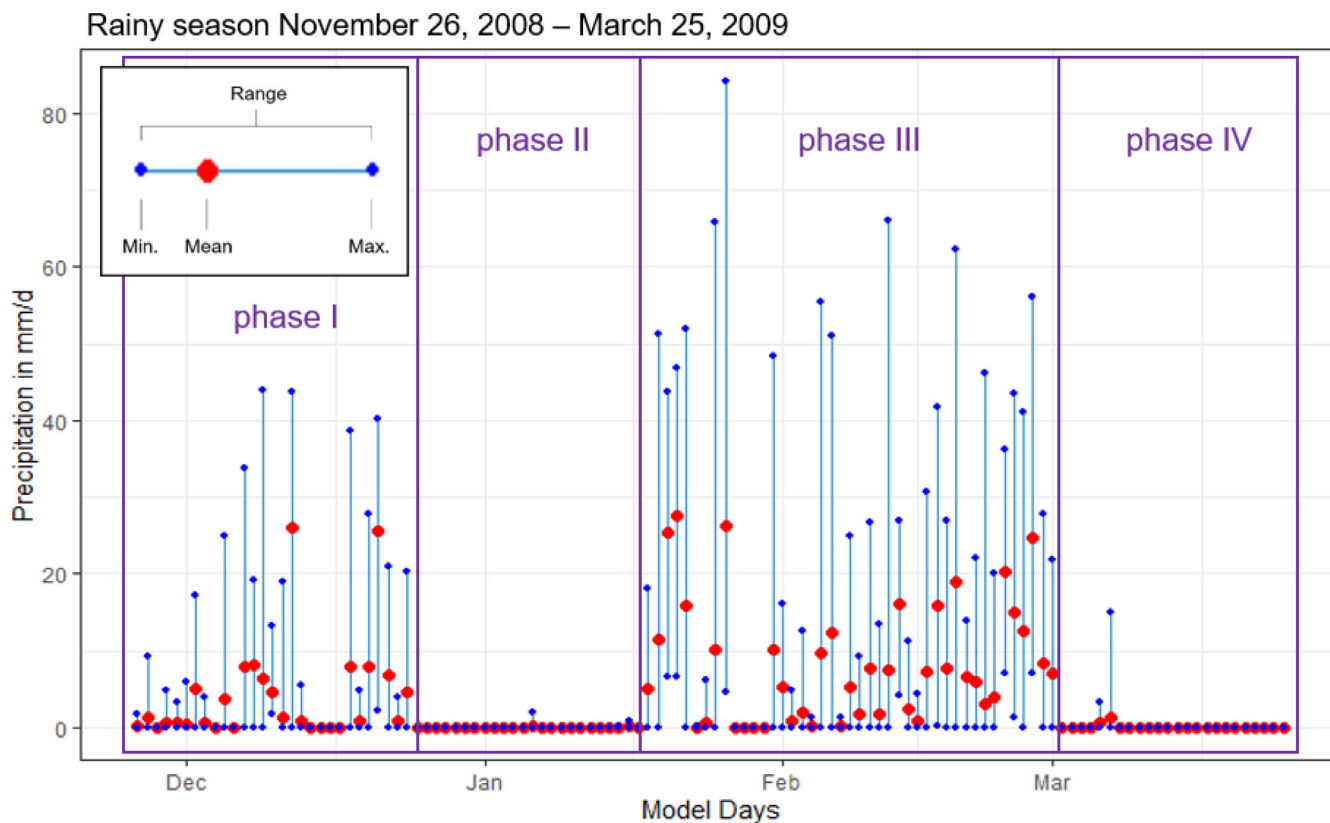


FIGURE 3 Summary statistics of the 15 TRMM precipitation raster cells covering the study area, including the four rainy and dry phases described in Section 3.1. [Color figure can be viewed at wileyonlinelibrary.com]

$$P_{\text{eff}} = \frac{(P - I_a)^2}{(P - I_a) + S_{0.1}} \quad (4)$$

S , potential retention; I_a , initial abstraction; λ , initial abstraction ratio; P , precipitation; P_{eff} , effective precipitation (Woodward et al., 2003, modified).

According to Woodward et al. (2003), a lower λ value of 0.1 was chosen to prevent an overestimation in runoff (Equation 3 and 4). As a first step, the hydrological soil groups (HSG) were extracted from the HYSOGs 250 m data set. This data set provides worldwide gridded hydrological soil groups for curve number-based runoff modeling (Ross et al., 2018). To match the TRMM precipitation tiles, the data set was aggregated by a majority filter in ArcGIS. With this method, each tile received its dominant HSG. Likewise, a supervised land use classification was used to extract the major cover types. Afterward, the curve numbers were calculated from USDA (2009) (Table 1).

To incorporate the different preconditions of soil wetness before each precipitation event, a further correction step was applied prior to every single simulation iteration. The antecedent soil moisture conditions (ASMCI) were categorized into three levels after the style of Sobhani (1975), which can be found in Verma et al. (2017) and can be seen in Table 1. With the SCS-CN method, the spatially distributed direct runoff for each time step was calculated and implemented in FloodArea.

2.5 | Evapotranspiration from water surfaces

If long periods and large areas are simulated in a study, evapotranspiration (ET) from the flowing water is an important factor that influences the model results. However, evaporation data are difficult to estimate for large basins with sparse observations. During the SASSCAL I (Southern African Science Service Centre for Climate Change and Adaptive Land Management) program many meteorological stations were installed in the study area (Helmschrot & Jürgens, 2015). However, data for potential evapotranspiration (ETp) are not available. Moreover, all of the stations were installed after the 2009 flood event. Alternatively, literature research provides information about estimated and measured ET and ETp values. A differentiation between these two terms is usually necessary during runoff formation, but when water evaporates from the river surface during the flow process, ET almost equals ETp. In an experiment on three different test sites in the Omusati region (north central Namibia), Kotani et al. (2017) quantified ET during the cultivation period with mean values ranging between 1.4 and 3.8 mm/d and maximum values of ET within a span of 5.4 to 11.2 mm/d. As one of the oldest values in literature, Cunningham et al. (1992) determined ETp from November to March in a range of 190 to 265 mm/month (6.1 to 9 mm/d). When downscaled to the exact time span of the model period, the ETp sum is 895 mm. Mendelsohn and Weber (2011) mention ETp sum of 760 mm from November to March with a daily mean ranging between

TABLE 1 List of applied curve numbers according to the specification of hydrological soil groups, land cover type, and hydrological condition for each precipitation tile. The CN values are further defined for each ASMC level from I to III (Antecedent Soil Moisture Condition).

Tile Nr.	1	2	3	4	5	6	7	8	9	10	11	12	13	14	15
HSG (Ross et al., 2018)	2 B	3 C	3 C	2 B	3 C	3 C	3 C	3 C	3 C	3 C	3 C	3 C	2 B	3 C	2 B
Cover Type (USDA, 2009)	BG ^a	BG ^a	BG ^a	PG ^b	BG ^a	BG ^a	BG ^a	PG ^b	PG ^b	PG ^b	PG ^b	PG ^b	PG ^b	PG ^b	PG ^b
Hydrological condition	Good	Good	Good	Good	Good	Good	Good	Good	Good	Good	Good	Good	Good	Good	Good
Curve Number (CN) according to HSG and cover type (USDA, 2009)	48	65	65	61	65	65	65	74	74	74	74	74	61	74	61
ASMC I	28	44	44	40	44	44	44	55	55	55	55	55	40	55	40
ASMC II	48	65	65	61	65	65	65	74	74	74	74	74	61	74	61
ASMC III	70	83	83	80	83	83	83	88	88	88	88	88	80	88	80

^aBG: Bush-brush-forbs-grass mixture with brush the major element.

^bPG: Pasture, grassland, or range continuous forage for grazing.

4.7 and 7.7 mm. Mendelsohn et al. (2013) sets 1062 mm for the same time, giving daily mean values from 7.0 up to 10.3 mm. Külls (2000) calculated ET with a Class A pan in Grootfontein southeast of the Etosha Pan. It resulted in a sum of 827 mm with daily means spanning between 3.8 and 8.4 mm/d (again downscaled to the model time). All research results have one aspect in common: they do not take into account the daily degree of cloud cover, which has a major impact in terms of ET, especially during the rainy season. Therefore, the work of Goormans et al. (2015) was referenced when considering ET. They use a pragmatic and engineering approach by assuming that ET is lower during precipitation events than afterward. Thus, they make the assumption that no ET is considered on days with more than 2 mm of precipitation and an ET of 8.5 mm must be considered on days with less than 2 mm of precipitation. When this was downscaled and applied to the model time frame and precipitation data, a total sum of 612 mm ET was calculated with daily differentiated ET values reflecting the individual amount of daily precipitation.

There is not an option to consider ET directly in FloodArea during the model run, so ET was subtracted afterward from the model output water depth layer (Figure 4).

3 | RESULTS

3.1 | Rainfall characteristics

For the description of the 2008/2009 rainy season flood dynamics, precipitation must first be examined in detail (Figure 4). It is noticeable that the precipitation can be segmented into 4 phases, which ultimately influence the runoff behavior: (1) The first phase lasted, with a small interruption, from the end of November to the end of December 2008 and was characterized by persistent precipitation; (2) this was followed by a phase of dry conditions that lasted until mid-January; (3) the second rain phase follows with longer-lasting and more intense rainfall than in the first phase. This phase was characterized by higher peak and daily precipitation values as well as higher average precipitation per day; (4) by the end of March, precipitation decreased, and runoff continued until the end of the model period on March 25, 2009.

With the onset of the rainy season in November/December 2008, precipitation occurred mainly in the west. One week later, precipitation also occurred in the northeast and east sections of the study area. At the same time, precipitation also affected areas north and south of Oshakati. The city surface remained dry at first.

3.2 | 2D-hydrodynamic model results

According to the rainfall characteristics, a diffuse picture of surface runoff emerges at the beginning of the modeling period, in which significant large-scale channel flow was not recognizable. Only from the 16th model day on (December 11, 2008) larger and coherent surface water areas become apparent in the central and northern area, most

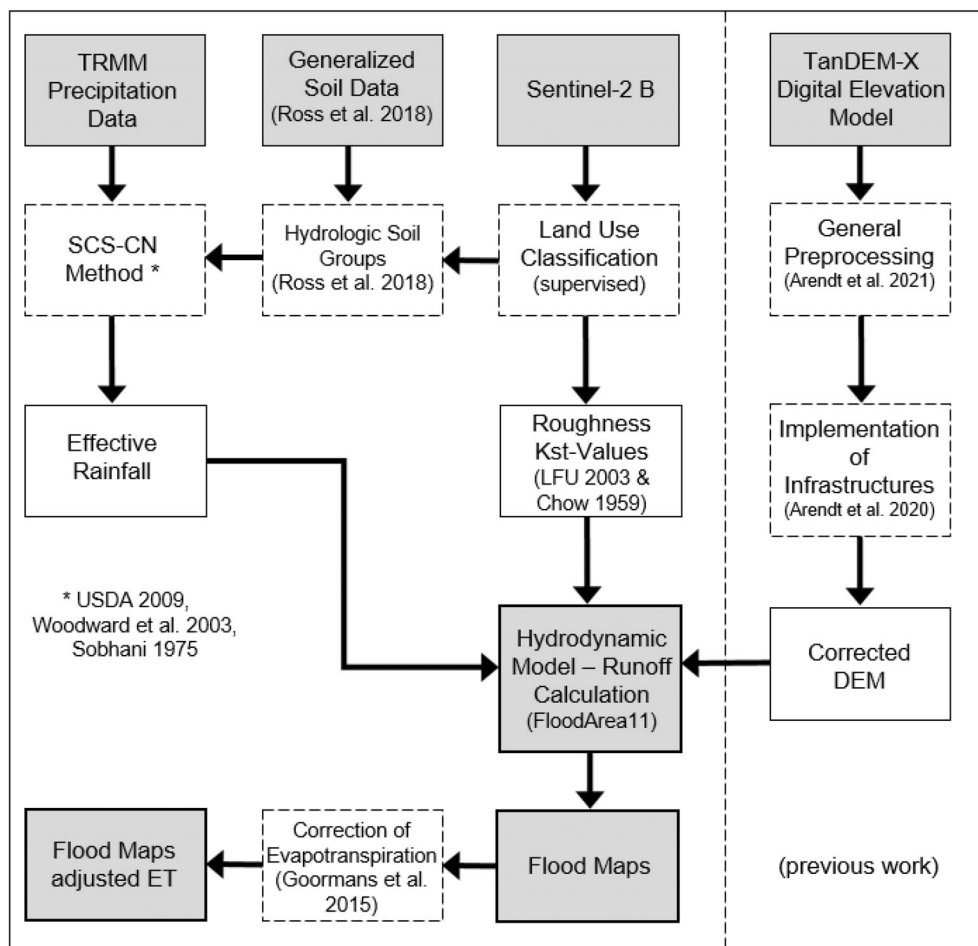


FIGURE 4 Process of data preparation and calculation. Gray boxes: model input/output data. Dashed boxes: processing steps. White boxes: intermediate products.

with a max. 0.2 m depth. By the end of the first precipitation phase at the 30th model day, interconnectivity, and flow processes between the individual lishana start to become visible (Figure 5 and Supporting Information).

The larger lishana and pans in the north, which were already filled at the beginning of the model period, continue to be filled. A main Oshana channel stands out very clearly, which runs from the northeast along the catchment boundary southward toward Oshakati. While it was wider in the northeast and filled with more water (depths up to 1 m), it becomes narrower in the southern course and was often filled with water only up to half a meter deep. This was joined by another smaller and more branched drainage channel coming from the central area. North of Oshakati, these streams fill the lishana and pans in and around the city. Water depths ranged from 0.1 m to 1 m.

In the second, rain-free phase, the surface water drained increasingly toward the south while, at the same time, it accumulates in deeper depressions. The first flow processes come to a standstill. In some lishana streams, interconnectivity is interrupted. Water levels generally drop to 0.2 to 0.5 m. The larger individual depressions in the central and northern areas retain surface runoff with a depth of 1 m.

The third phase (second rain phase) begins with heavy rainfall. First, the smaller, but prominently discernible, west-southwest running lishana stream is reactivated, and the precipitation water flows in

a channelized manner westward past Oshakati to the south. A few days later, persistent precipitation also leads to increased accumulation of larger volumes of water in the pans in the central area (Angola). A similar pattern was observed in the northwest. The lishana and pans overflow and reconnect with each other. Distinct flow processes were evident. The lishana strand fed by the northern and central pans brings large volumes of water toward Oshakati. This was further enhanced by the eastern lishana strand, which carries the largest volumes of water at this time. On model Day 94 (February 27, 2009), the greatest water depths and widest inundations was reached (Figures 5 and A1).

Particularly large, deep, and isolated lishana (Figure 6[1]), as well as borrow pits and interconnected lishana, show very-high water levels since no overflowing has taken place yet. At some locations, water levels ranging from 2 to 5 m were reached. In some borrow pits, the water level also rises to over 5 m. At this point, the average water levels in the ephemeral systems were between 0.5 and 1.5 m.

Crossing the border region between Angola and Namibia, lishana channels become narrower and take on the pattern of nearly straight lines. Due to the slender morphology of the channels, shallow bank overflows occur in some places with water depths of 0.1 to 0.2 m (Figure 6[2]).

For Oshakati and the surrounding areas (Figure 6[3]) channel overflow leads to larger flooding, including backwater effects in

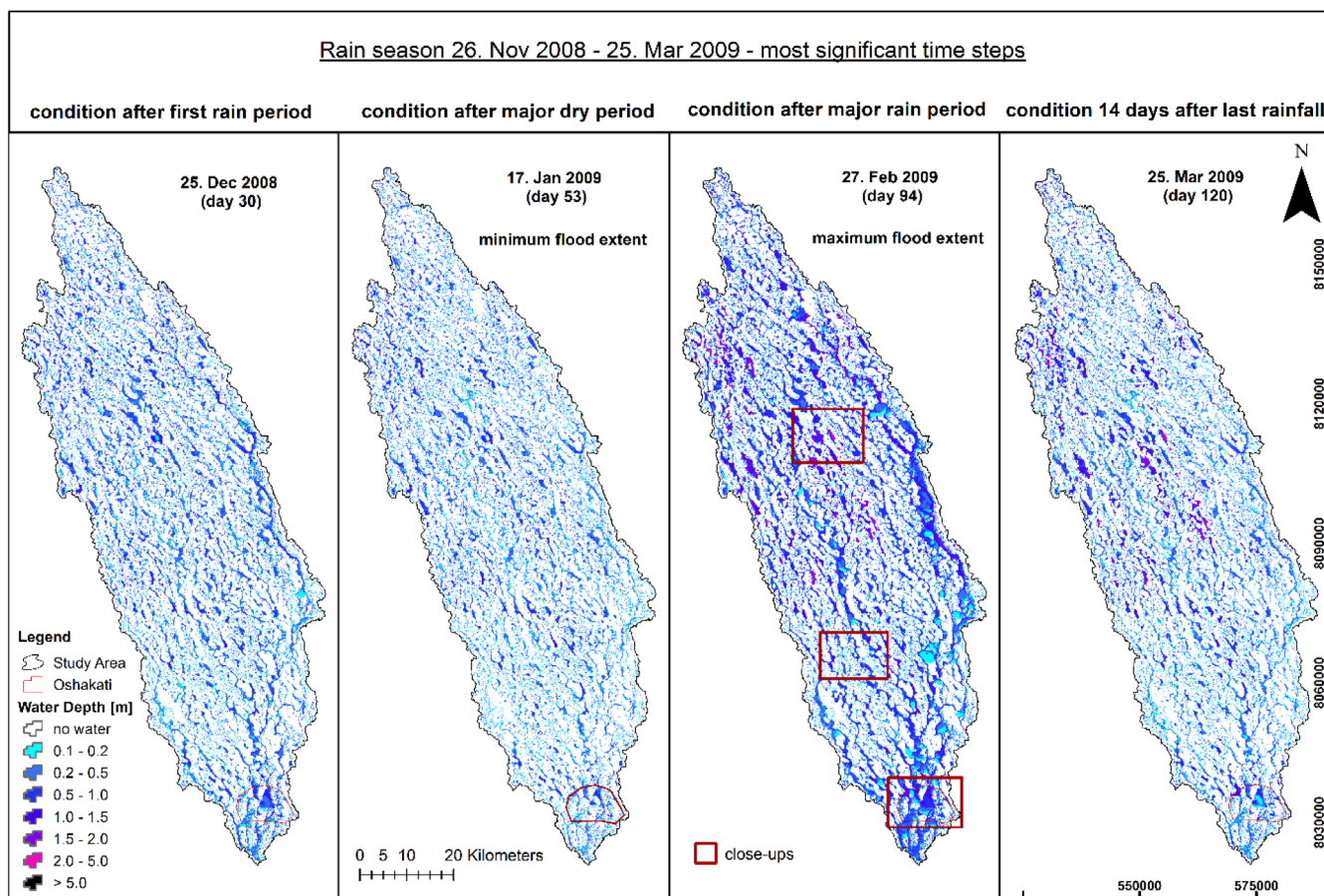


FIGURE 5 Four most significant time steps of inundation during the rainy season from November 2008 to March 2009. An enlarged version can be seen in Figure A1. [Color figure can be viewed at wileyonlinelibrary.com]

topographically flat and urban areas. In these flood events, shallow depths of 0.1 to 0.2 m were observed. The estimated flow velocities in the study area were between 0.15 and 0.35 m/s. In particularly narrow channel areas, flow velocities of about 0.5 m/s were reached. The respective flow velocities were impacted on the one hand by the respective local gradient and on the other hand by obstructions, such as transverse structures (road dams and embankments).

On March 07, 2009, the last precipitation fell during the rainy season (model day 102). March 25, 2009 was chosen as the final day to be evaluated, 14 days after the last rainfall event. In the picture rendered for this day, it can be clearly seen that the surface water flow between the lishana were mostly disconnected. This was particularly noticeable on the southwestern lishana strand. The city of Oshakati also experiences minimal flow from the northeast. Most parts of the city were largely dry, and water were again concentrated in its original channel beds. Larger sections were now flooded only between 0.1 and 0.2 m in very shallow areas.

In the northern part of the catchment (Angola), wide and deep pans continued to retain larger amounts of water. On the Namibian side, some unconnected lishana also remained as water reservoirs, while others ran dry. South of Oshakati, there was no longer a backwater and the waters have drained further south toward the Lake

Oponono area. At this point, the total discernible water volume was about 0.547 km³.

In addition, the water level variation (stage hydrographs) over the model runtime was observed at three different locations in the study area (Figures 6 and 7). Specifically, observations were made in the close-up areas (Figure 6) at the virtual stage hydrographs locations pointed out in the model.

The three hydrographs (Figure 7) also confirm the above-mentioned runoff behavior in the region, as well as the effects of the periods without precipitation. The course of the surface runoff from north to south, the fast runoff of the water through the central areas of the drainage system as well as the larger and longer-lasting water quantities in the Angolan part were evident.

3.3 | Evapotranspiration

Figure 8 compares two selected time steps, showing the study area with ET from the water surfaces according to Goormans et al. (2015) and comparing it with images of raw model data without ET (see Supporting Information). The first-time step compares water levels and maximum inundation at the end of the first (rainfall) phase on January

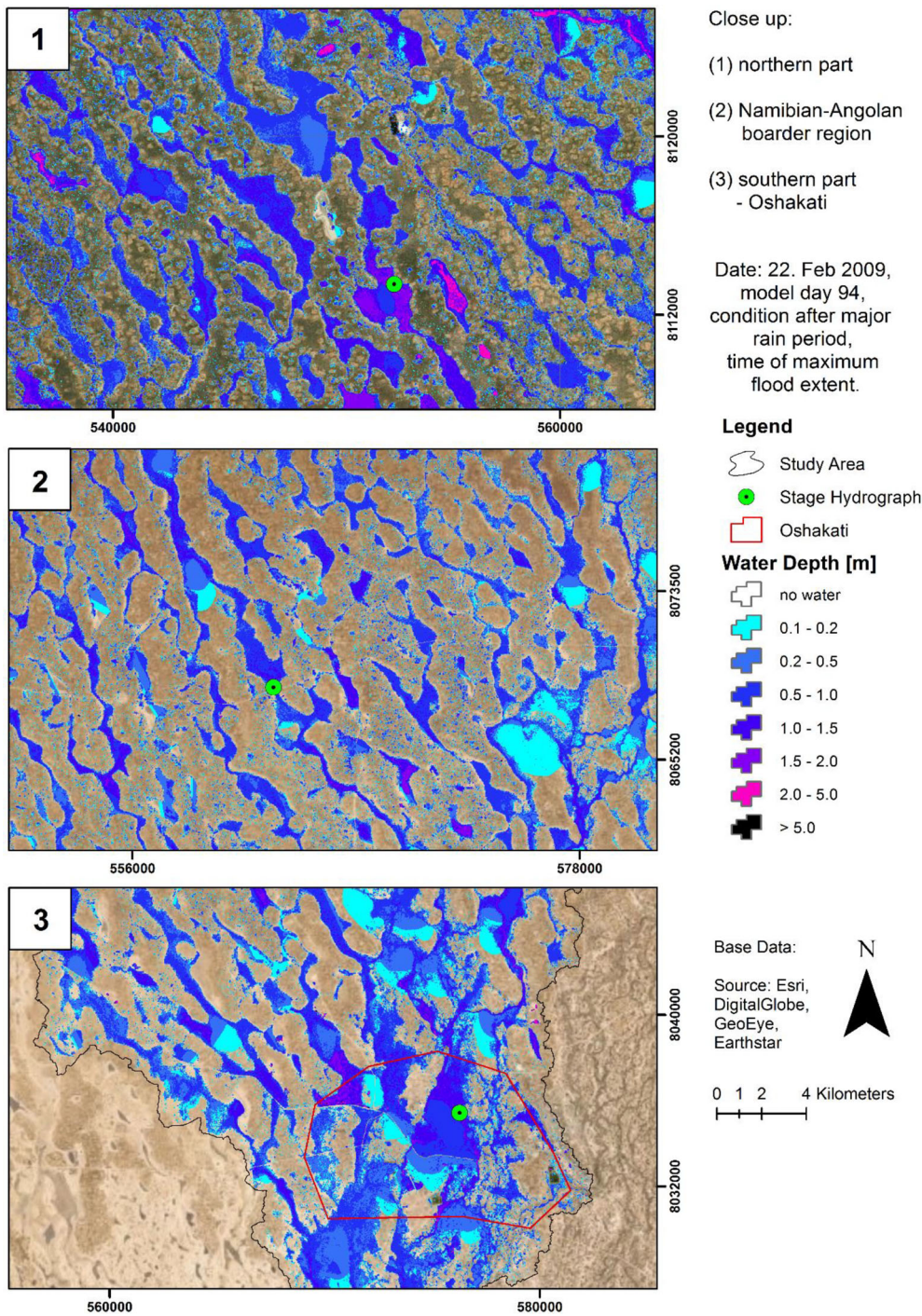


FIGURE 6 Close up of three representative inundation areas from the northern, central, and southern part of the study area (location see Figure 5). [Color figure can be viewed at wileyonlinelibrary.com]

17, 2009 (model day 53). The first image does not include ET while the second includes an ET of 450.5 mm to date.

The next two images on the right (Figures 8 and A2) compare the dry weather runoff at the end of the rainy season on March 25, 2009. One image shows no ET, and the other was generated with a total ET of 612 mm.

Without the inclusion of ET, the conditions after the major rain periods show more extensive flooding. In the model, heavy flooding and backwater effects were clearly visible. However, with the consideration of 450.5 mm ET, backwater effects no longer existed, except

for some smaller parts in Oshakati. Moreover, interconnectivity and continuous flow processes were interrupted. The phenomenon of discontinuity on an Oshana mainstream in the southwest of the basin was clearly evident.

The model comparison of the runoff on March 25 including and excluding ET shows large differences in water volume (Figures 8 and A2). This figure (right sub-figure) depicting the effects of ET, the interconnection and flow processes were completely interrupted. Only larger and deeper pans retained water. The flood event appeared to be over and the lishana were no longer overflowing.

The water volumes between the two right sub-figures for March 25 (Figures 8 and A2) differ by a factor of 4.7. If ET is not included, the surface water volume amounts to 0.547 km³, while including ET with 612 mm results in a reduced amount of surface water, lowering it to a volume of 0.116 km³.

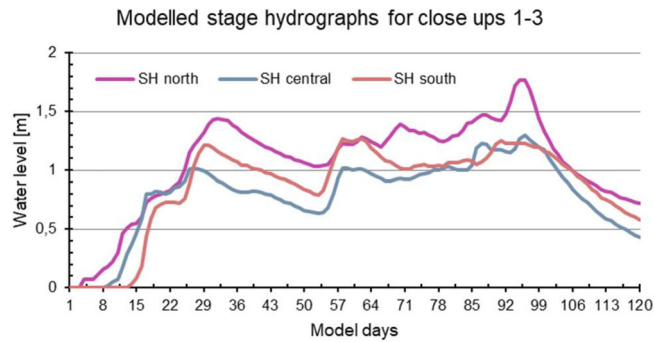


FIGURE 7 Virtual stage hydrographs over time of the model period for three different close-up regions mentioned in Figures 5 and 6. SH north = stage hydrograph in close up 1; SH central = stage hydrograph in close up 2; SH south = stage hydrograph in close up 3. [Color figure can be viewed at wileyonlinelibrary.com]

4 | DISCUSSION

4.1 | Model results and reference data

Because of a lack of discharge and water level observations, only a tentative evaluation of the model outputs can be done based on the maximum extent of flooded areas extracted from satellite images. During the rainy season, with its dense and frequent cloud cover, optical satellite data do not provide sufficient information and the extraction of flooded areas for specific dates was not possible. Therefore, to provide at least an estimate of the real flooding conditions, a combination of optical and radar satellite data provided by L. Beck (see Arendt et al., 2021 for details) was used. The data of the multi-temporal analysis represent a cumulative image in which every pixel was marked that was identified as being covered with water for at least 1 day between October 2008 and September 2009.

The comparison of model outputs with the reference data set is shown in Figures 8 and A2. The overlapping results are also symbolized in green. Accordingly, the spatial distribution of the flooded area corresponds to a match of 100% between the model result and the multi-temporal satellite image analysis (Figures 9 and A3).

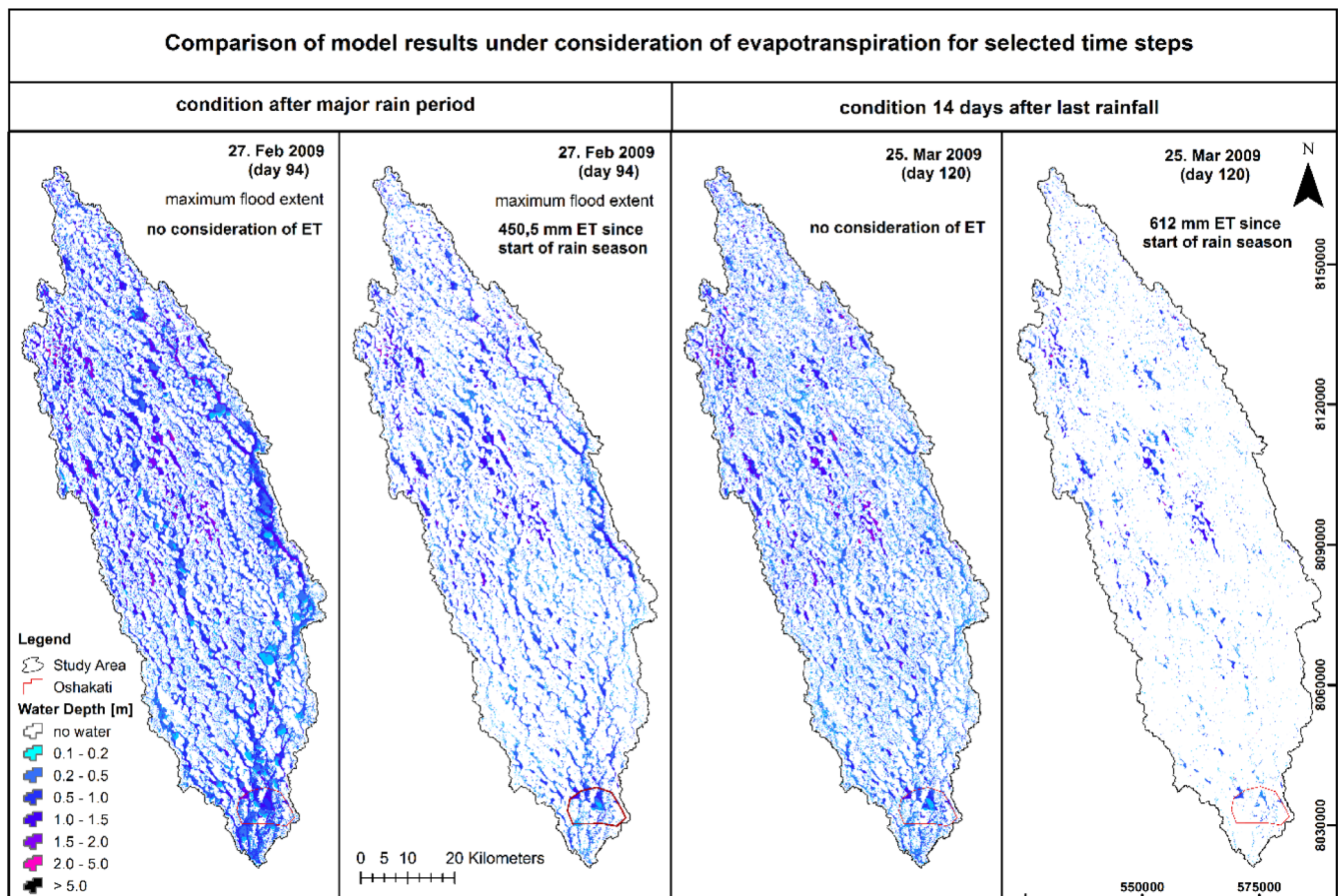


FIGURE 8 Comparison of the model results including and excluding evapotranspiration. An enlarged version can be seen in Figure A2. Also watch for the Supporting Information. [Color figure can be viewed at wileyonlinelibrary.com]

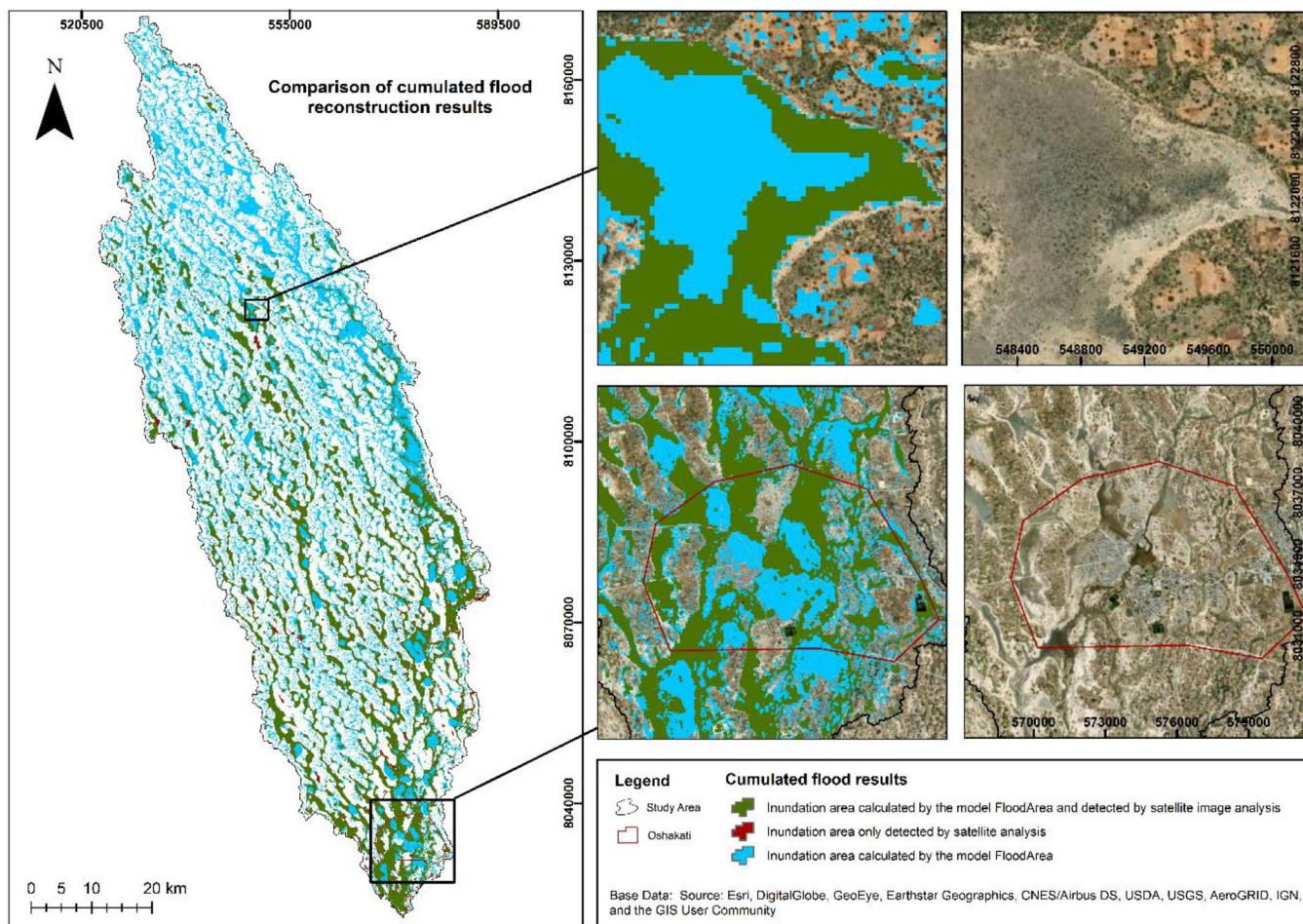


FIGURE 9 Comparison of simulation results with the reference water mask. Green: Areas flooded in model and reference data; Blue: Flooding in the model only; Red: Flooded areas only in the reference mask. An enlarged version can be seen in Figure A3. [Color figure can be viewed at wileyonlinelibrary.com]

The cumulative inundation area $>0.1 \text{ m}^2$ amounts to about 1860 km^2 according to the calculation with FloodArea. In contrast, the size of the inundation area derived from the satellite images is almost 3 times smaller, measuring only 673 km^2 in size. An agreement between model and reference data can be achieved for 620 km^2 only, which is surprisingly low. However, this effect must be attributed to the limitations of the reference data rather than a general lack of model performance.

It is noticeable that the overlap of the results varies spatially according to the application of the two different methods. Thus, there are far more overlapping areas in the southern part of the study area than there are in the northern part. One reason for the difference in detection is due to the different methods and how they deal with land use. In Figures 9 and A3, a closer examination of the northern example area (both upper right images) shows that the hydrodynamic model was able to capture the water flow in its natural path according to the channel hydraulics and other parameters. The analysis of the satellite images, on the other hand, has problems at this point in distinguishing shallow water areas, dark soils, and vegetation. As a result, inundation was greatly underestimated. In particular, the northern

(Angolan) part of the study area was much more vegetated and characterized by larger shrubs and contiguous clusters of trees. Another obstacle in multi-sensor analysis is the different spatial resolutions behind it. For example, at coarser resolutions, smaller water areas cannot be recorded and are incorrectly classified as dry. The same can be true for urban areas, in whose narrower streets the water is not detected, and the reflectance of the roofs dominates. The resulting mixed pixel effect, which is also associated with the too-coarse resolution, makes it difficult to classify the area as flooded (see Figures 9 and A3, both image sections, bottom right). If we assume that the hydrodynamics were simulated correctly, the strong overestimation of the flooded areas would be a further result of the limited representation of water surface evaporation. Evaporation plays a central role in the semi-arid study area and significantly influences the model results.

4.2 | Intricacy of evapotranspiration

However, as described in the section on evaporation (2.5.), there was little to no area-wide evaporation data available. To completely

disregard evaporation leads to a significantly overestimated result. The approach of Goormans et al. (2015) corrects the result, but it also leads to an overestimation of ET. It becomes apparent that the real inundated area was something between the two calculated results in Figure 8 comparing no ET and 612 mm of ET.

Everything indicates that an overestimation of evaporation losses occurred. A new model run with adjusted ET values could remedy this situation. One possibility would be to calculate with the even lower values provided by Külls (2000).

4.3 | Differences between Angola and Namibia

Noteworthy in the results of the work presented here was the large water reservoirs in the central part of the study area and in the north-east and east of the Angolan territory. Some smaller amounts also remain visible in the border area. In the Namibian area, smaller reservoirs can only be identified in the south around the city of Oshakati. The picture of excessive ET losses therefore shows a clear difference in the remaining water volumes between the north (Angola) and the south (Namibia). The reasons for these differences are minor morphological variations and an increased total precipitation on the Angolan side.

4.4 | Surface runoff behavior

Nevertheless, these data provide excellent insights into the spatial-temporal distribution of water volumes, their surface runoff behavior, and thus the interconnectivity of the lishana system. In the simulation, three main streamlines could be identified, through which the water volumes rapidly discharged toward the south. Two of the three join on the Namibian side and subsequently flow through the city of Oshakati and are thus of particular safety relevance with respect to the regional capital. Furthermore, it can be seen that there are larger water bodies on the Angolan side. Close to the Angolan-Namibian border, network structures with individual isolated depressions and pans in between become visible. Further south, the system becomes more diversified again. Throughout the study area, individual large areas flooded to a depth of only 0.1 m were repeatedly identified. These do not correspond completely with comparative data and were likely due to the correction of the digital terrain model. Accordingly, it was an overestimation of the amount of water because these areas have been leveled too much, leaving water on them.

5 | CONCLUSIONS AND OUTLOOK

This study conducted a transferable 2D-hydrodynamic modeling approach of the region around the lishana system in the Culvelai Basin for the first time ever. The used FloodArea model is based on a single high spatial resolution (25 × 25 m) TanDEM-X digital terrain model. It covers a long and continuous model period of 120 days while using

temporally and spatially varying TRMM precipitation data. As a result, flood routing could be performed in addition to data on inundation surfaces, depths, and volumes at different times. In addition, a volume balance of the remaining and available water at the end of the rainy season could be determined.

Not considering ET leads to an obviously overestimated value of 0.547 km³ water remaining while the application of ET results in an underestimated value of 0.116 km³. The true picture might be found somewhere in between. The same problem also applies to the calculation of floodplains, which, neglecting ET, was around 1860 km². Here, too, this was clearly an overestimated value. Nevertheless, by means of these calculations, three main streams could be identified, two of which join further south and drain through Oshakati. All three streams discharge the water visibly fast. This provides an important indication of a possible safety hazard, especially for the regional capital. In addition, the calculations show that the net-like connectivity of the lishana system becomes increasingly tighter toward the center of the study area, revealing numerous isolated depressions. In the southern area, the picture again becomes more diffuse. Water depths range from 0.1 m to 14 m, with all areas deeper than 5 m attributed to borrow pits. On average, the water depth was about 0.2 m.

These findings have high socio-political value. Although the ET data are not yet conclusive and needs to be improved in further work, the study successfully demonstrates how surface water flows through the lishana system during a rainy season and provides important initial indications of flow paths, water volumes, and velocities. These new findings help to better understand the interconnected system, answer questions about the distribution of water and its quantity and identify hazards.

Therefore, the model can be used for scenario calculations of future floods. An important goal of further work should be to use the knowledge gained here for the implementation of flood protection and water storage measures, as well as to use synergy effects in order to preserve and increase water resources, even throughout pronounced drought periods.

ACKNOWLEDGMENTS

We are grateful for the financial support by the Department of Earth Science, Freie Universität Berlin. We thank the German Aerospace Centre (© DLR 2017) for their delivery and support with the TanDEM-X data (Proposal ID: DEM_HYDR1285). We also express gratitude to Dr. Sandro Martinis, Dr. Tobias Ullmann, and Lorenz Beck for their support with evaluation data. The German Hydrological Society (DHG) supported this work with a scholarship. Open Access funding enabled and organized by Projekt DEAL.

CONFLICT OF INTEREST STATEMENT

The authors declare no competing interests.

DATA AVAILABILITY STATEMENT

The data that support the findings of this study are openly available in Refubium at <http://dx.doi.org/10.17169/refubium-35737>.

ORCID

Robert Arendt  <https://orcid.org/0000-0002-2200-5895>

REFERENCES

- Achleitner, S., Huber, A., Lumassegger, S., Kohl, B., Spira, Y., & Weingraber, F. (2020). *Pilot Study Upper Austria. Modeling of pluvial floods in response to heavy precipitation events. Guidance for practitioners.* [https://www.interreg-central.eu/Content.Node/Home/Projects/RAINMAN/Main-Project-outputs-/RAINMAN-LeitfadenEN-V1.0-20200623-\(1\).pdf](https://www.interreg-central.eu/Content.Node/Home/Projects/RAINMAN/Main-Project-outputs-/RAINMAN-LeitfadenEN-V1.0-20200623-(1).pdf)
- Arendt, R., Faulstich, L., Jüpner, R., Assmann, A., Lengricht, J., Kavishe, F., & Schulte, A. (2020). GNSS mobile road dam surveying for TanDEM-X correction to improve the database for floodwater modeling in northern Namibia. *Environmental Earth Science*, 79(333), 1–15. <https://doi.org/10.1007/s12665-020-09057-5>
- Arendt, R., Reinhardt-Imjela, C., Schulte, A., Faulstich, L., Ullmann, T., Beck, L., ... Lengricht, J. (2021). Natural pans as an important surface water resource in the Cuvelai Basin—Metrics for storage volume calculations and identification of potential augmentation sites. *Water*, 13(2), 177. <https://doi.org/10.3390/w13020177>
- Ata, R. (2017). Telemac 2D (Version 7.2) [User manual]. http://www.opentelemac.org/downloads/MANUALS/TELEMAC-2D/telemac-2d_user_manual_en_v7p0.pdf
- Awadallah, A. G., & Tabet, D. (2015). Estimating flooding extent at high return period for ungauged braided systems using remote sensing: A case study of Cuvelai Basin, Angola. *Natural Hazards*, 77, 255–272. <https://doi.org/10.1007/s11069-015-1600-6>
- Bischofberger, J., Schuldt-Baumgart, N., & Lenzen, E. (2016). *Omeya Ogo Omwenyo—Water is Life*. CuveWaters Report. Frankfurt/Main, Germany: ISOE. <https://doi.org/10.13140/RG.2.1.2287.7047>
- Bradbrook, K. (2006). JFLOW: A multiscale two-dimensional dynamic flood model. *Water and Environment Journal*, 20, 79–86. <https://doi.org/10.1111/j.1747-6593.2005.00011.x>
- Chow, V. T. (1959). *Open-channel hydraulics*. McGraw-Hill, Civil Engineering Series.
- Cunningham, T., Auino, E., Marsh, A., & Seely, M. (1992). *Oshanas: Sustaining people, environment, and development in central Owambo, Namibia*. DRFN.
- De Groeve, T. (2010). Flood monitoring and mapping using passive microwave remote sensing in Namibia. *Geomatics, Natural Hazards and Risk*, 1(1), 19–35. <https://doi.org/10.1080/19475701003648085>
- Desalegn, H., & Mulu, A. (2021). Mapping flood inundation areas using GIS and HEC-RAS model at Fetam River, Upper Abbay Basin Ethiopia. *Scientific African*, 12, e00834. <https://doi.org/10.1016/j.sciaf.2021.e00834>
- Faulstich, L., Schulte, A., Arendt, R., Kavishe, F., & Lengricht, J. (2018). Die Qualität der intensiv genutzten Oberflächengewässer im Cuvelai-Becken (Nord-Namibia) zum Ende der Trockenzeit 2017. In P. Chiffard, D. Karthe, & S. Möller (Eds.), *Beiträge zum 49. Jahrestreffen des Arbeitskreises Hydrologie* Symposium conducted at the meeting of Arbeitskreis Hydrologie, Göttingen, Germany.
- Filali-Meknassi, Y., Ouarda, T. B. M. J., & Wilcox, C. (2014). *Data access, availability and quality assessment for the development of a flood forecasting model for Namibia*. UNESCO.
- Gaughan, A. E., Staub, C. G., Hoell, A., Weaver, A., & Waylen, P. R. (2016). Inter- and intra-annual precipitation variability and associated relationships to ENSO and the IOD in southern Africa. *International Journal of Climatology*, 36, 1643–1656. <https://doi.org/10.1002/joc.4448>
- geomer GmbH. (2017). *FloodAreaHPC-Desktop (Version 10.3) [User manual]*. https://www.geomer.de/fileadmin/downloads/produkte/software/floodarea/2018_UserManualFloodArea10.pdf
- Goormans, T., van Looveren, R., Mufeti, P., & Wynants, J. (2015). Building a hydrological and hydrodynamic model while facing challenges in data availability in the Oshana region of central northern Namibia. In A. Mynett (Ed.), *E-proceedings of the 36th IAHR world congress*. The Netherlands.
- Goudie, A., & Viles, H. A. (2015). *Landscapes and landforms of Namibia*. Springer.
- Helmschrot, J., & Jürgens, N. (2015). Integrated SASSCAL research to assess and secure current and future water resources in southern Africa. *Proceedings of the International Association of Hydrological Sciences*, 366, 168–169. <https://doi.org/10.5194/piahs-366-168-2015>
- Hipondoka, M. H. T. (2005). *The development and evolution of Etosha pan* (Doctoral dissertation). Julius-Maximilians-University. urn:nbn:de:bvb:20-opus-14351
- Hüser, K., Besler, H., Blümel, W. D., Heine, K., Leser, H., & Rust, U. (2001). *Namibia: Eine Landschaftskunde in Bildern*. Klaus Hess Verlag.
- Kerdiles, H., Rembold, F., & Pérez-Hoyos, A. (2015). *Seasonal monitoring in Namibia. Ad hoc report. Severe drought affecting cereal production and pastoral areas in northern and Central Namibia*. Joint Research Centre of the European Union http://the-eis.com/elibrary/sites/default/files/downloads/literature/Seasonal%20Monitoring%20in%20Namibia_2015.pdf
- Kluge, T., Liehr, S., Lux, A., Moser, P., Niemann, S., Umlauf, N., & Urban, W. (2008). IWRM concept for the Cuvelai Basin in northern Namibia. *Physics and Chemistry of the Earth, Parts ABC*, 33(1–2), 48–55. <https://doi.org/10.1016/j.pce.2007.04.005>
- Kotani, A., Hiyama, T., Ohta, T., Hanamura, M., Kambatuku, J. R., Awala, S. K., & Iijima, M. (2017). Impact of rice cultivation on evapotranspiration in small seasonal wetlands of north Central Namibia. *Hydrological Research Letters*, 11(2), 134–140. <https://doi.org/10.3178/hr.11.134>
- Külls, C. (2000). *Groundwater of the North-Western Kalahari, Namibia. Estimation of recharge and quantification of the flow system* (Doctoral thesis). Julius-Maximilians-University.
- Kundzewicz, Z. W., Kanae, S., Seneviratne, S. I., Handmer, J., Nicholls, N., Peduzzi, P., ... Sherstyukov, B. (2013). Flood risk and climate change: Global and regional perspectives. *Hydrological Science Journal*, 59(1), 1–28. <https://doi.org/10.1080/02626667.2013.857411>
- Leandro, J., Chen, A. S., & Schumann, A. (2014). A 2D parallel diffusive wave model for floodplain inundation with variable time step (P-DWave). *Journal of Hydrology*, 517, 250–259. <https://doi.org/10.1016/j.jhydrol.2014.05.020>
- Luetkemeier, R., Stein, L., Drees, L., & Liehr, S. (2017). Blended drought index: Integrated drought Hazard assessment in the Cuvelai-Basin. *Climate*, 5(3), 51. <https://doi.org/10.3390/cli5030051>
- Mandl, D., Frye, S., Sohlberg, R., Cappelaere, P., Handy, M., & Grossman, R. (2013). The Namibia Early Flood Warning System, a CEOS pilot project. *Proceedings of the 2012 IEEE International Geoscience and Remote Sensing Symposium*, Munich, Germany. <https://doi.org/10.1109/IGARSS.2012.6350660>
- Manning, R. (1891). On the flow of water in open channels and pipes. In *Institution of civil engineers of Ireland* (Vol. XX, pp. 161–207). Transactions of the Institution of Civil Engineers of Ireland. <https://doi.org/10.48495/r207ts96k>
- Mendelsohn, J., & Weber, B. (2011). *Cuvelai: The Cuvelai Basin, its Water and People in Angola and Namibia = Povos e águas da bacia do Cuvelai em Angola e Namibia* (Occasional paper). https://www.angonet.org/dw/sites/default/files/online_lib_files/CUVELAI%20BASIN%20-%20BACIA%20DO%20CUVELAI.pdf
- Mendelsohn, J. M., Jarvis, A., & Robertson, T. (2013). *A profile and atlas of the Cuvelai-Etosha Basin*. RAISON and Gondwana Collection.
- Mufeti, P., Rientjes, T., Mabande, P., & Maathuis, B. (2013). Application of a satellite based rainfall-runoff model: A case study of the Trans Boundary Cuvelai Basin in Southern Africa. In Ouwehand, L. (Ed.), *Proceedings of the European Space Agency Living Planet Symposium*, Edinburgh, UK.
- Müller, I., Hipondoka, M., Winkler, K., Geßner, U., Martinis, S., & Taubenböck, H. (2018). Monitoring flood and drought events—Earth

- observation for multiscale assessment of water-related hazards and exposed elements. *Biodiversity & Ecology*, 6(6), 136–143. <https://doi.org/10.7809/b-e.00315>
- Ngula Niipele, J., & Chen, J. (2019). The usefulness of alos-palsar dem data for drainage extraction in semi-arid environments in the Ilishana sub-basin. *Journal of Hydrology: Regional Studies*, 21, 57–67. <https://doi.org/10.1016/j.ejrh.2018.11.003>
- Nujić, M. (2016). HYDRO_AS-2D-2D-Strömungsmodell für die wasserwirtschaftliche Praxis. Benutzerhandbuch, Version 4.2.1. In Hydrotec Ingenieurgesellschaft für Wasser und Umwelt mbH (Ed.), September 2016, Rosenheim.
- Persendt, F. C., & Gomez, C. (2016). Assessment of drainage network extractions in a low-relief area of the Cuvelai Basin (Namibia) from multiple sources: LiDAR, topographic maps, and digital aerial orthophotographs. *Geomorphology*, 260, 32–50. <https://doi.org/10.1016/j.geomorph.2015.06.047>
- Persendt, F. C., Gomez, C., & Zawar-Reza, P. (2015). Identifying hydro-meteorological events from precipitation extremes indices and other sources over northern Namibia, Cuvelai Basin. *Jambá*, 7(1), 177. <https://doi.org/10.4102/jamba.v7i1.177>
- Reason, C. J. C., & Smart, S. (2015). Tropical south East Atlantic warm events and associated rainfall anomalies over southern Africa. *Frontiers in Environmental Science*, 3(24), 1–11. <https://doi.org/10.3389/fenvs.2015.00024>
- Rizzoli, P., Martone, M., Gonzalez, C., Wecklich, C., Borla Tridon, D., Bräutigam, B., ... Huber, M. (2017). Generation and performance assessment of the global TanDEM-X digital elevation model. *ISPRS Journal of Photogrammetry and Remote Sensing*, 132, 119–139. <https://doi.org/10.1016/j.isprsjprs.2017.08.008>
- Ross, W. C., Prihodko, L., Anchang, L., Kumar, S., Ji, W., & Hanan, N. P. (2018). Data descriptor: HYSOGs250m, global gridded hydrologic soil groups for curve-number-based runoff modeling. *Scientific Data*, 5(150091), 1–8. <https://doi.org/10.1038/sdata.2018.91>
- Seely, M., Henderson, J., Heyns, P., Jacobson, P., Nakale, T., Nantanga, K., & Schachtschneider, K. (2003). Ephemeral and endoreic river systems: Relevance and management challenges. In A. Turton, P. Ashton, & E. Cloete (Eds.), *Transboundary Rivers, sovereignty and development: Hydropolitical drivers in the Okavango River basin* (pp. 187–212). AWIRU.
- Shifidi, V. T. (2016). Impact of flooding on rural livelihoods of the Cuvelai Basin in northern Namibia. *Journal of Geography and Regional Planning*, 9(6), 104–121. <https://doi.org/10.5897/JGRP2015.0536>
- Skakun, S., Kussul, N., Shelestov, A., & Kussul, O. (2013). Flood Hazard and flood risk assessment using a time series of satellite images: A case study in Namibia: Flood Hazard and flood risk assessment. *Risk Analysis*, 34(8), 1521–1537. <https://doi.org/10.1111/risa.12156>
- Sobhani, G. (1975). *A review of selected small watershed design methods for possible adoption to Iranian conditions* (Master's thesis). Utah State University.
- Strickler, A. (1923). Beiträge zur Frage der Geschwindigkeitsformel und der Rauheitszahlen für Ströme, Kanäle und geschlossene Leitungen (contributions concerning the question of the flow velocity formula and roughness values for streams, channels and conduits). *Mitteilungen Des Amtes für Wasserwirtschaft*, 16, 77.
- Tarboton, D. G. (1997). A new method for the determination of flow directions and upslope areas in grid digital elevation models. *Water Research*, 33(2), 309–319. <https://doi.org/10.1029/96WR03137>
- Tyrna, B., Assmann, A., Fritsch, K., & Johann, G. (2018). Large-scale high-resolution pluvial flood hazard mapping using the raster-based hydrodynamic two-dimensional model FloodAreaHPC. *Journal of Flood Risk Management*, 11(1), 1024–S1037. <https://doi.org/10.1111/jfr3.12287>
- United States Department of Agriculture (USDA). (2009). Hydrologic Soil Groups. In United States Department of Agriculture (USDA) (Eds.), *National Engineering Handbook Part 630 Hydrology* (7).
- Van Der Waal, B. (1991). Fish life of the Oshana Delta in Owambo, Namibia, and the translocation of Cunene species. *Madoqua*, 17, 201–209.
- Verma, S., Verma, R. K., Misha, S. K., Singh, A., & Jayaraj, G. K. (2017). A revisit of NRC-CN inspired models coupled with RS and GIS for runoff estimation. *Hydrological Sciences Journal*, 62(12), 1891–1930. <https://doi.org/10.1080/02626667.2017.1334166>
- Wendleder, A., Wessel, B., Roth, A., Breunig, M., Martin, K., & Wagenbrenner, S. (2013). TanDEM-X water indication mask: Generation and first evaluation results. *IEEE Journal of Selected Topics in Applied Earth Observations and Remote Sensing*, 6(1), 171–179. <https://doi.org/10.1109/JSTARS.2012.2210999>
- Wessel, B. (2016). *TanDEM-X Ground Segment—DEM Products Specification Document* (Public Document TD-GS-PS-0021, Issue 3.1). Oberpfaffenhofen, Germany: EOC, DLR.
- Woodward, D. E., Hawkins, R. H., Jiang, R., Hjelmfelt junior, A. T., Van Mullem, J. A., & Quan, D. Q. (2003). *Runoff curve number method: examination of the initial abstraction ratio*. Paper presented at the 2003 World Water and Environmental Resources Congress, Philadelphia. [https://doi.org/10.1061/40685\(2003\)308](https://doi.org/10.1061/40685(2003)308)
- Zimmermann, M. (2013). *Sustainable Transformations of Water Supply Regimes—The Cuvelai-Etoshia Basin in Central Northern Namibia* (Schriftenreihe IWAR 224). Technische Universität Darmstadt, TUprints website: https://tuprints.ulb.tu-darmstadt.de/3737/1/Zimmermann_Dissertation.pdf

SUPPORTING INFORMATION

Additional supporting information can be found online in the Supporting Information section at the end of this article.

How to cite this article: Arendt, R., Reinhardt-Imjela, C., Faulstich, L., Schulte, A., Assmann, A., Jüpner, R., Johannes, P. T., & Mashauri, D. A. (2023). Hydrodynamic modeling of ephemeral flow in the Ilishana channel systems of the Cuvelai Basin—Northern Namibia. *River Research and Applications*, 39(9), 1902–1918. <https://doi.org/10.1002/rra.4187>

APPENDIX A

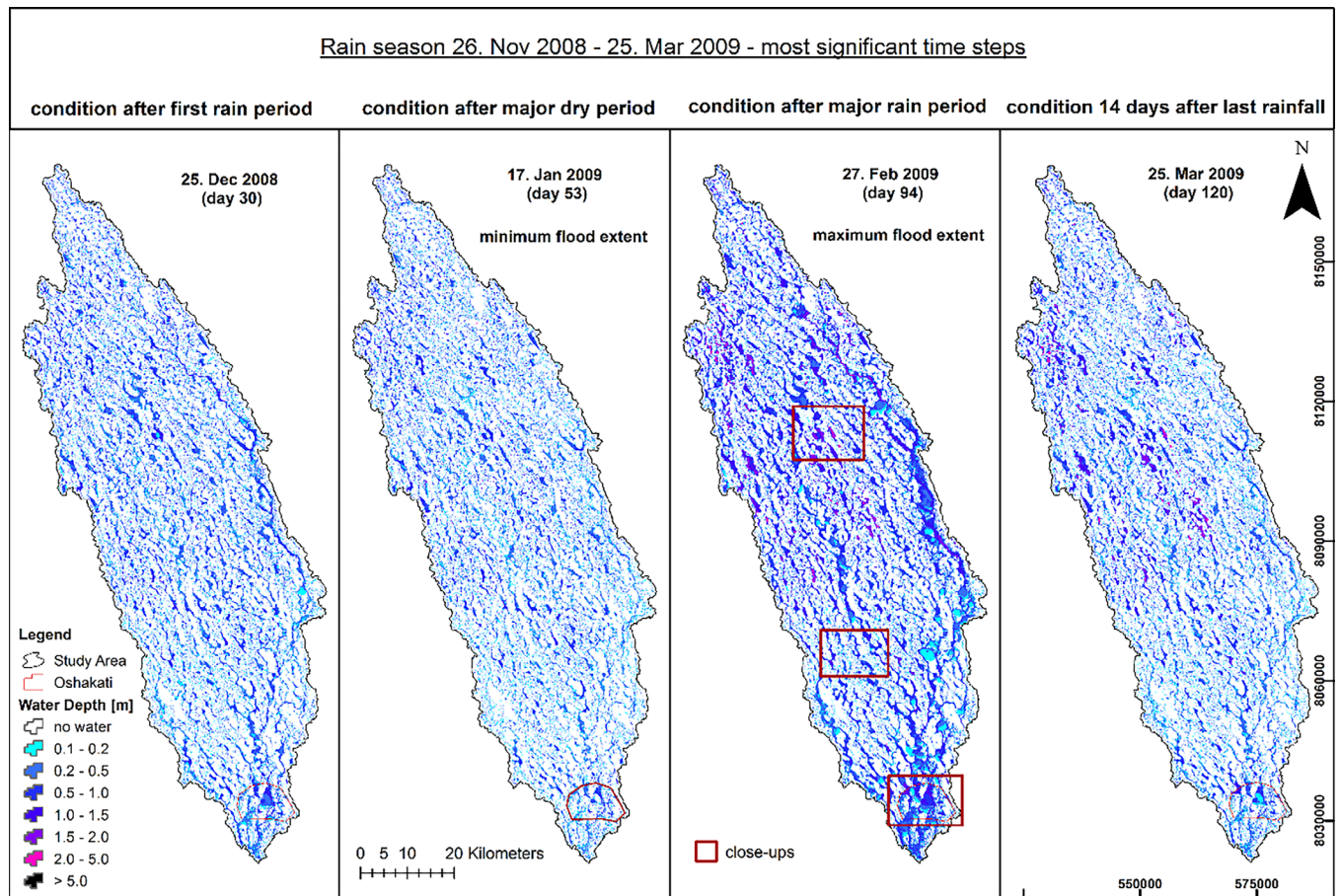


FIGURE A1 Four most significant time steps of inundation during the rainy season from November 2008 to March 2009 (enlarged version of Figure 5). [Color figure can be viewed at wileyonlinelibrary.com]

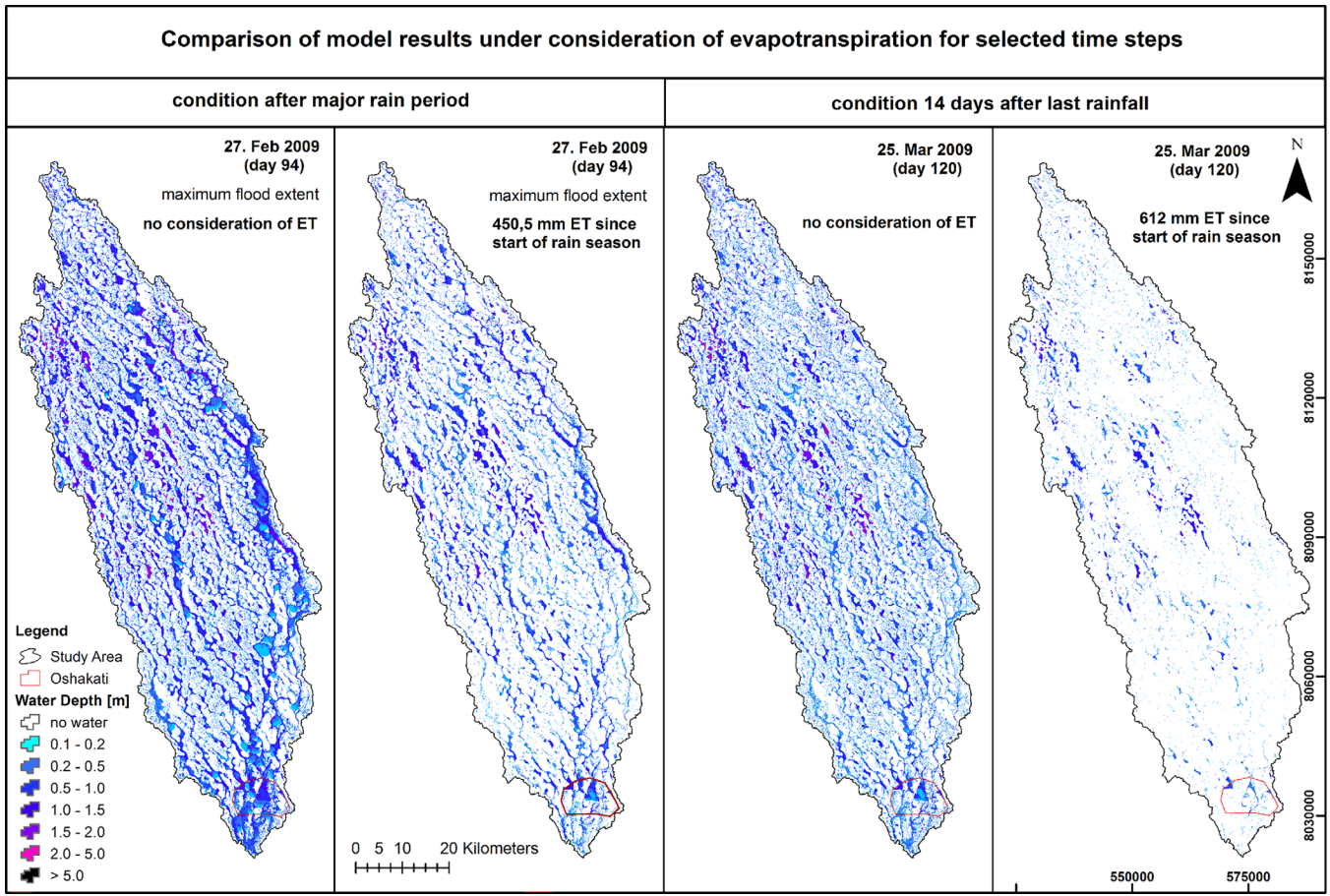


FIGURE A2 Comparison of the model results including and excluding evapotranspiration (enlarged version of Figure 8). [Color figure can be viewed at wileyonlinelibrary.com]

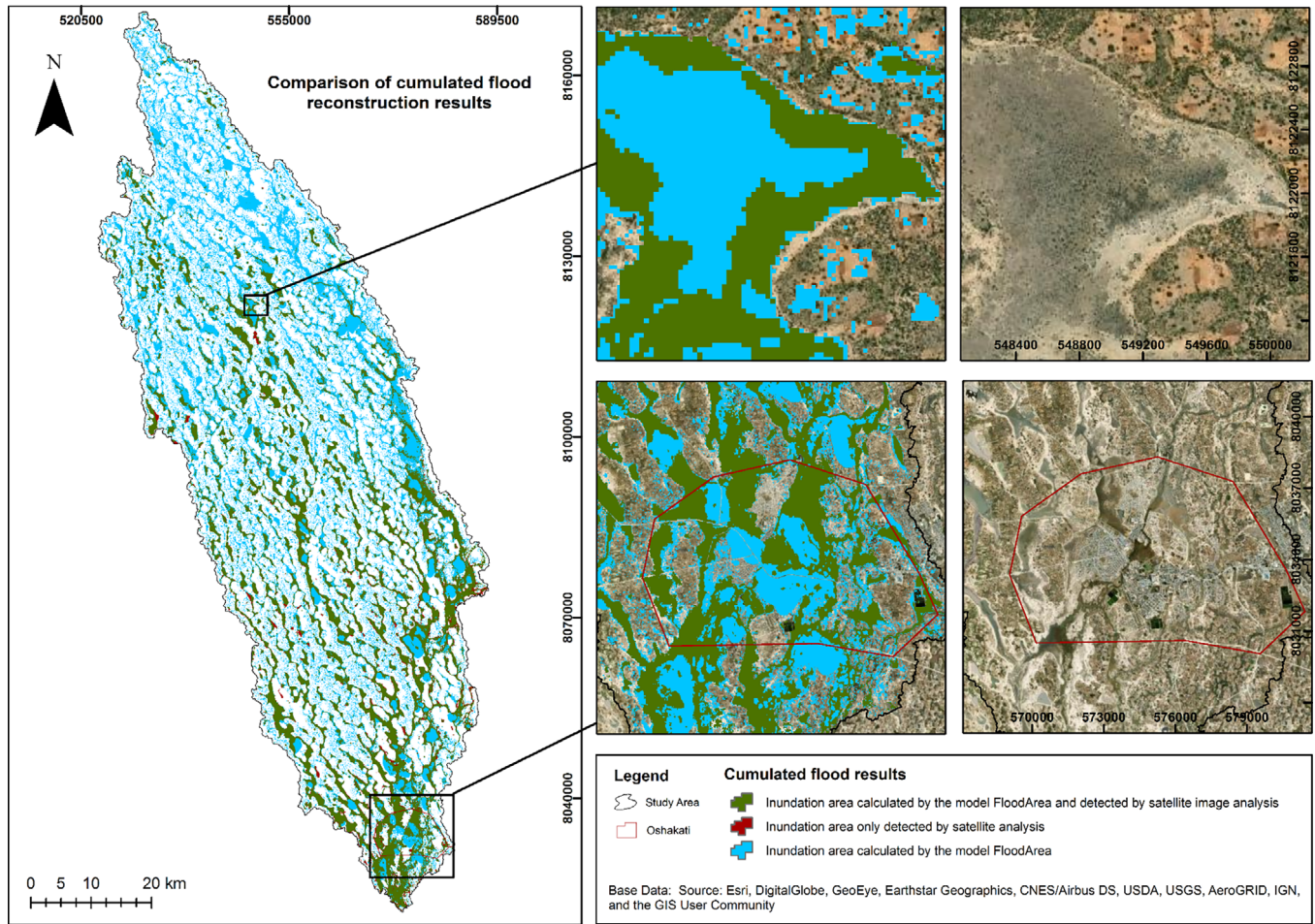


FIGURE A3 Comparison of simulation results with the reference water mask. Green: Areas flooded in model and reference data; Blue: Flooding in the model only; Red: Flooded areas only in the reference mask (enlarged version of Figure 9). [Color figure can be viewed at wileyonlinelibrary.com]